

Article

Spin Current Enhancement Using Double-Ferromagnetic-Layer Structure for Magnetoelectric Spin-Orbit Logic Device

Bayartulga Ishdorj, Shumaila Sharif and Taehui Na * 

Department of Electronics Engineering, Incheon National University, Incheon 22012, Republic of Korea; tulga5111@gmail.com (B.I.); shumaila.sharif@inu.ac.kr (S.S.)

* Correspondence: taehui.na@inu.ac.kr; Tel.: +82-32-835-8452

Abstract: The use of Moore's law appears to be coming to an end due to technological and physical constraints, as complementary metal-oxide semiconductor (CMOS) transistors become smaller and closer to the atomic scale. Therefore, various emerging technologies are being researched as potential successors to traditional CMOS transistors, and one of the most exciting candidates is the magnetoelectric spin-orbit (MESO) device. The MESO device comprises two portions (input and output) and it cascades charge/voltage as input and output signals. In the MESO device's output portion, ferromagnetic (FM) and high-spin-orbit-coupling layers are employed to provide spin-polarized current and charge/voltage output. In this paper, we offer a description and analysis of the operating mechanism of the MESO device's output portion using a spin flow approach and propose a double-FM-layer structure. In the double-FM-layer structure, we implement two FM layers with antiparallel magnetization directions, instead of using a single-FM-layer structure to increase the output charge/voltage. The proposed structure is verified through the Verilog-A compact model.

Keywords: beyond CMOS; magnetoelectric spin-orbit (MESO) device; spintronic device; spin polarization; spin-orbit coupling (SOC)



Citation: Ishdorj, B.; Sharif, S.; Na, T. Spin Current Enhancement Using Double-Ferromagnetic-Layer Structure for Magnetoelectric Spin-Orbit Logic Device. *Electronics* **2024**, *13*, 4085. <https://doi.org/10.3390/electronics13204085>

Academic Editors: Francis Balestra and Gerard Ghibaudo

Received: 27 August 2024

Revised: 4 October 2024

Accepted: 16 October 2024

Published: 17 October 2024



Copyright: © 2024 by the authors. Licensee MDPI, Basel, Switzerland. This article is an open access article distributed under the terms and conditions of the Creative Commons Attribution (CC BY) license (<https://creativecommons.org/licenses/by/4.0/>).

1. Introduction

Gordon E. Moore first noted a long-term tendency in technological node scaling 59 years ago, and this finding has served as a fundamental driver in the semiconductor industry's explosive growth and transformation. Although there have been significant advances in process technology, design methodologies, and architectural innovations over the past six decades, the task of scaling technology nodes has become increasingly difficult due to a multitude of physical, technical, and engineering challenges. Predicting the ultimate limit of Moore's law is particularly challenging due to numerous interrelated factors, but quantum physics may define the boundaries of electronic miniaturization and processing capabilities in the future [1]. Given this scenario, it is both logical and imperative that we investigate and develop novel beyond-CMOS options to sustain and maintain the accelerated growth of digital information processing systems. Currently, various types of physical quantities are being explored for potential use in beyond-CMOS devices to encode information effectively, and one of the most promising among these is the spin state of electrons [2–6]. Utilizing spin as the state variable instead of traditional charge carriers holds significant prospects, including reduced power consumption, faster operational speeds, improved scalability, and non-volatility. A notable advancement in this field is magnetoelectric spin-orbit (MESO) logic, which represents the latest generation of beyond-CMOS spintronics devices, effectively harnessing these advantages to pave the way for more efficient and powerful computing technologies [5].

As shown in Figure 1, the MESO device is divided into two major portions: input and output. The input portion of the MESO device utilizes magnetoelectric (ME) material (e.g., BiFeO₃) to enable the low-energy magnetic state switching of the ferromagnet (FM). The

output portion of the MESO device utilizes high-spin-orbit-coupling material to translate the datum encoded in the magnetic orientation of the FM into a charge/voltage output, achieved through the inverse spin-orbit coupling (ISOC) effect [7–10]. The ISOC effect facilitates the use of charge-based signal transmission across logic stages, circumventing concerns, like the spin diffusion length typically associated with all-spin logic [11] relying on the spin current for signal transport.

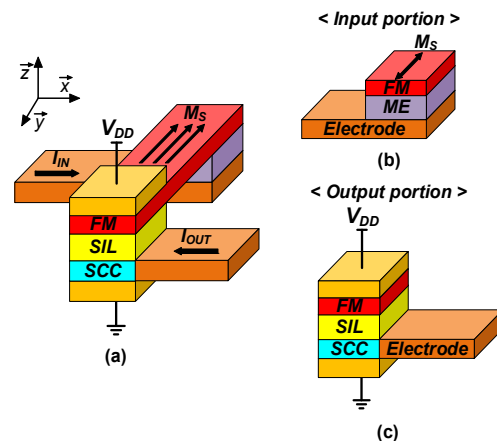


Figure 1. MESO device. (a) Structure of the MESO device. (b) Input portion of the MESO device. (c) Output portion of the MESO device.

While the MESO device exhibits promise as a viable beyond-CMOS logic solution, unlocking its full potential depends on further advancements in MESO at the material and device level. Previous device level research on MESO has primarily concentrated on the input portion and circuit modeling [12–14]. Consequently, we posit that a focus on comprehending and developing the output portion of the MESO device is necessary at this point.

In this research, we thoroughly describe and analyze the operating mechanism of the output component of the MESO device, employing a spin flow approach. Furthermore, we propose an innovative double-FM-layer structure with the aim of enhancing device performance. The efficacy of this proposed structure is validated through mathematically accurate Verilog-A compact model-based SPECTRE simulations, which allow us to assess the dynamics and operational characteristics of the MESO device in detail.

In Section 2, we provide a comprehensive review of the existing structures and technologies related to the MESO device. We also introduce our spin-flow-based explanation of its operating mechanism, emphasizing the importance of the spin polarization and conversion processes. Section 3 is dedicated to a detailed introduction of the double-FM-layer structure of the MESO device, where we explain its configuration and the rationale behind the design choices.

In Section 4, we present the setup of, and results derived from, our simulations, showcasing the performance metrics and validating the effectiveness of our proposed structure. Finally, we conclude our study in Section 5, summarizing the key findings and discussing the implications of our work for future developments in MESO technology. This comprehensive approach not only contributes to the understanding of the MESO device's operational principles but also highlights the potential for advancements in spintronic applications.

2. Review of the Existing Structure

2.1. Operating Mechanism of the Input Portion of MESO

To facilitate the practical application of the MESO device, it is imperative to formulate a clear and accessible explanation of the underlying physical effects that constitute its functionality.

(1) Magnetoelectric (ME) effect: The input mechanism of the MESO device initiates with the ME layer. ME is a multiferroic material that has both ferromagnetic and ferroelectric orders, as demonstrated in Figure 2, enabling the control of polarization of ME by applying a magnetic field or the manipulation of the magnetization of the ME through an electric field—a phenomenon known as the ME effect [15–17]. When the charge/voltage input is supplied to the ME layer through an electrode connected to the bottom side, it induces a potential difference between the top and bottom sides of the ME layer, thereby resulting in the electric-field-induced magnetization switching of the ME layer. It should be noted that, given that the primary function of the ME layer involves generating an electric field, it can be conceptualized and modeled as a capacitor.

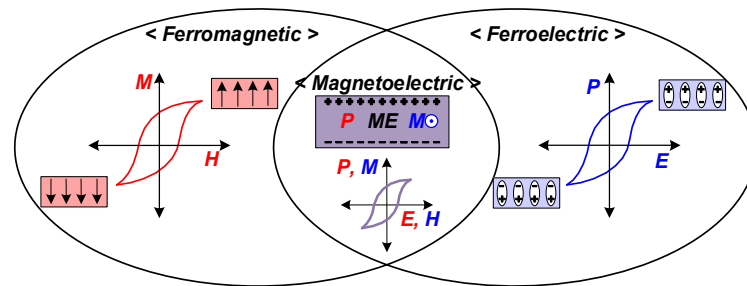


Figure 2. Schematic representation of magnetoelectricity and magnetoelectric material.

(2) Exchange bias: The control of the magnetic properties of the FM stands as the pivotal aspect of the MESO device, achieved by the electric-field-modulated exchange bias instigated by the ME layer at the interface of the FM and ME layers [18]. In simpler terms, this process involves the shifting of the hysteresis loop of the FM along the field axis, as shown in Figure 3, enabling the storage of computing data within the magnetic state of the FM. This capability underscores the MESO device’s potential for efficient data encoding and retention.

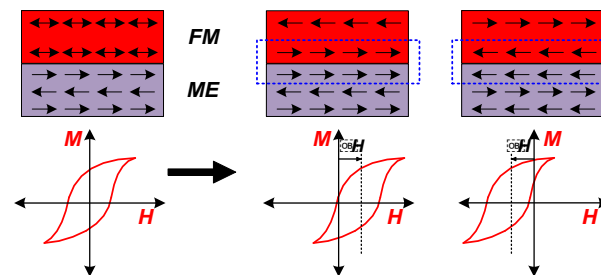


Figure 3. Exchange bias between FM and ME layers.

2.2. Operating Mechanism of the Output Portion of MESO

The output mechanism of the MESO device relies on two primary spin-based mechanisms. First, as the supply current (I_{supply}) flows through the ferromagnetic (FM) layer, spin polarization occurs depending on the magnetization direction of the FM layer. In this process, spin-polarized currents are created by aligning the spins of the charge carriers in a particular direction, influenced by the magnetic orientation of the FM layer. As shown in Figure 4, an unpolarized current represents a flow of carriers without any preferred spin orientation, while a spin-polarized current indicates that the majority of the carriers have their spins aligned in a specific direction. Essentially, a spin-polarized current encompasses both charge and spin components, and by leveraging the FM layer, it is possible to control or manipulate the spin orientation of the current.

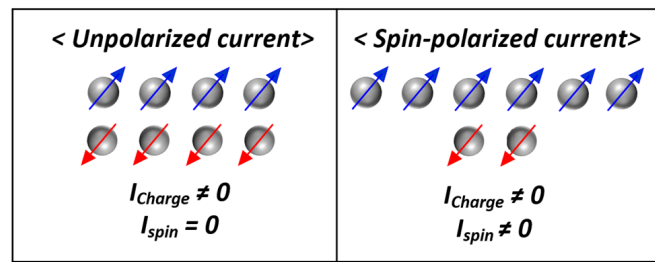


Figure 4. Illustration comparing an unpolarized current and a spin-polarized current.

Second, when this spin-polarized current is injected into a material with a high spin-orbit coupling, a spin-to-charge conversion occurs, producing a charge or voltage output. The efficiency of this spin-to-charge conversion is crucial in maximizing the device's performance and ensuring sufficient output levels for logic operations. Accurately modeling this spin conversion process is key to advancing MESO technology, especially as it aims to offer a viable alternative to CMOS devices.

To support the development of these emerging technologies, having an accurate yet simplified model is essential. As a result, we developed a spin-flow-based mechanism to describe the output portion of the MESO device, providing a clearer understanding of its operational dynamics. This model offers insights into how the interplay between the spin and charge components can be optimized to enhance the output efficiency and drive future innovations in spintronic devices.

In addition to the two main mechanisms, the spin injection layer plays a crucial role in the operation of the MESO device. It ensures the efficient conversion of charge/voltage signals into spin signals, allowing the cascading of spin-polarized currents necessary for logic operations. By injecting spin-polarized electrons, the layer drives magnetization switching in the ferromagnetic components, facilitating binary state transitions.

Figure 5 illustrates the operational mechanism of the MESO device's output section, elucidated through a spin-flow-based model. The operational mechanism of the output portion of the MESO device unfolds across two stages.

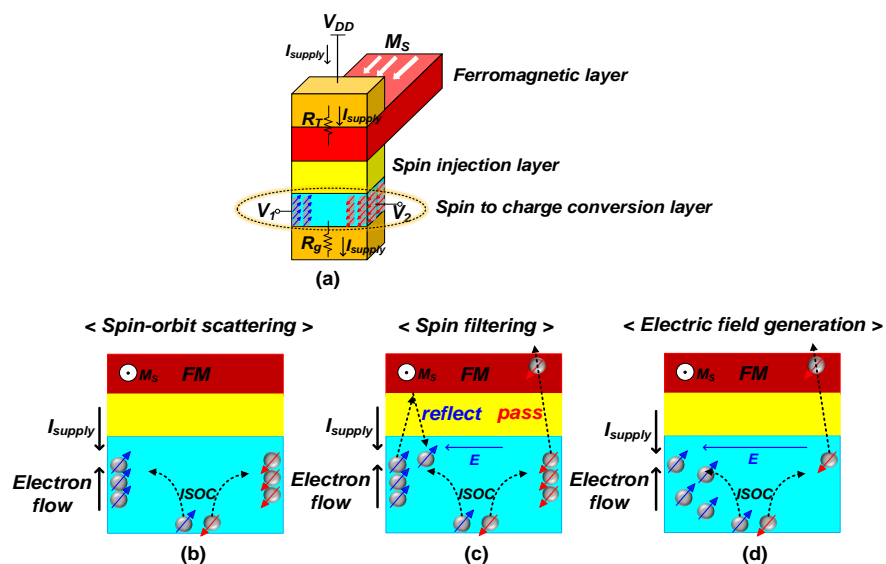


Figure 5. Processes of the output structure of the MESO device. (a) Output portion of the MESO. (b) Spin-orbit scattering. (c) Spin filtering. (d) Electric field generation.

Initially, as I_{supply} initiates a flow, conduction electrons begin to traverse from the ground to the spin-to-charge-conversion (SCC) layer. Within the SCC layer, impurities cause spin-orbit scattering, with up-spin electrons preferentially scattering in one direction

and down-spin electrons preferentially scattering in the opposite direction, as depicted in Figure 5b.

Simultaneously, spin-based filtering occurs at the interface between the spin injection layer and the FM layer, as depicted in Figure 5c. Conduction electrons possessing spins aligned with the FM layer traverse through, while those with spins not aligned are reflected back to the spin injection layer and the SCC layer. Note that, in this context, the spin-based filtering mechanism serves as the explanatory framework for the spin polarization observed within the I_{supply} .

Consequently, the combined effects of spin-orbit scattering and spin-based filtering result in an accumulation of electrons on one side of the SCC layer, creating a potential gradient within the SCC layer. Depending on the data encoded in the FM, a negative or positive potential difference between the V_1 and V_2 of the SCC layer is generated. As a result, either discharging or charging occurs at the output.

2.3. Circuit Modeling

A circuit model for MESO devices was initially proposed in [19], and more recent works have introduced alternative approaches and refinements to its circuit modeling [12–14]. The charge-equivalent circuit model for a single MESO device, shown in Figure 6, consists of several key components. The ferroelectric capacitor represents the magnetoelectric (ME) layer, which plays a pivotal role in controlling the switching mechanism of the device. Additionally, resistive elements account for the behavior of the spin-charge conversion (SCC) layer and the interconnects within the device. Specifically, the total resistance of the SCC layer is modeled by R_{SCC} , while R_{IC} captures the resistive effects of the interconnects. To further break down the SCC layer's resistances, the horizontal and vertical resistances are separately represented by $R_{\text{SCC},h}$ and $R_{\text{SCC},v}$, respectively, reflecting the anisotropic nature of spin transport within the device.

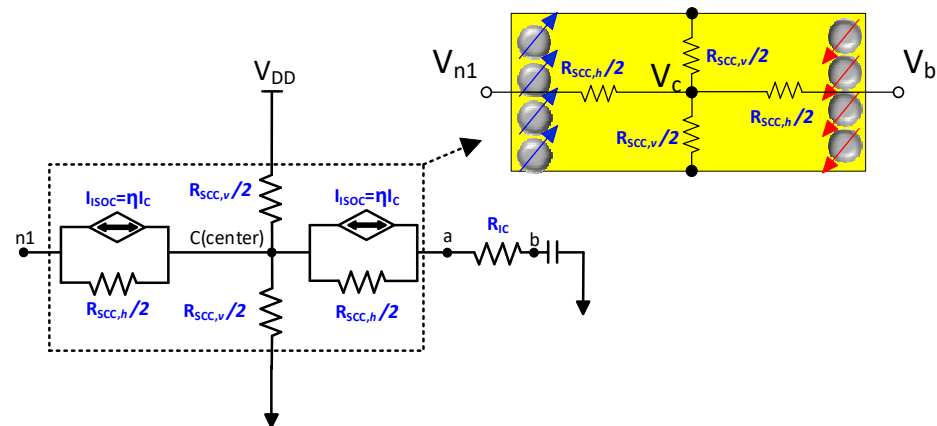


Figure 6. Circuit schematics of an MESO.

An important feature of the model is the current-controlled current source, which includes an internal resistance of $R_{\text{SCC},h}/2$, designed to simulate the process of spin-to-charge conversion. This element is crucial, because the conversion from spin-polarized current into charge/voltage output forms the basis of MESO operation. Efficient spin-to-charge conversion is directly linked to the overall device performance, including the output voltage and energy efficiency.

However, as highlighted in [5,12], achieving switching at low voltages remains a significant challenge, largely due to material limitations and the complex interplay between resistive elements in the circuit. This has prompted ongoing efforts to improve both the material properties and the device structure. In particular, the output charge/voltage of the MESO model is heavily influenced by key parameters such as the spin-to-charge conversion ratio (η) and the resistances of the SCC layer. Increasing the spin-to-charge conversion

efficiency η , and optimizing $R_{\text{SCC},h}$ and $R_{\text{SCC},v}$ can lead to substantial improvements in device performance. Specifically, increasing $R_{\text{SCC},h}$ while reducing $R_{\text{SCC},v}$ would raise the output charge/voltage, enhancing the MESO's utility as a low-power, high-efficiency logic element.

The proposed double-FM-layer structure represents a device-level effort to improve the output voltage of the MESO.

3. Double-FM-Layer Structure for MESO Device

Compatibility with CMOS logic is crucial in beyond-CMOS devices. Hence, increasing the output voltage of the MESO device is of paramount importance. One of the most direct methods of enhancing the output voltage is by augmenting the degree of spin polarization, which is defined as

$$P = \frac{(N_{\uparrow} - N_{\downarrow})}{(N_{\uparrow} + N_{\downarrow})} \quad (1)$$

where N_{\uparrow} and N_{\downarrow} represent the densities of up-spins and down-spins, respectively [20].

We propose a double-FM-layer structure for the output section of the MESO device, with the aim of enhancing its charge/voltage output by improving the efficiency of spin filtering. Figure 7a shows the proposed double-FM-layer structure.

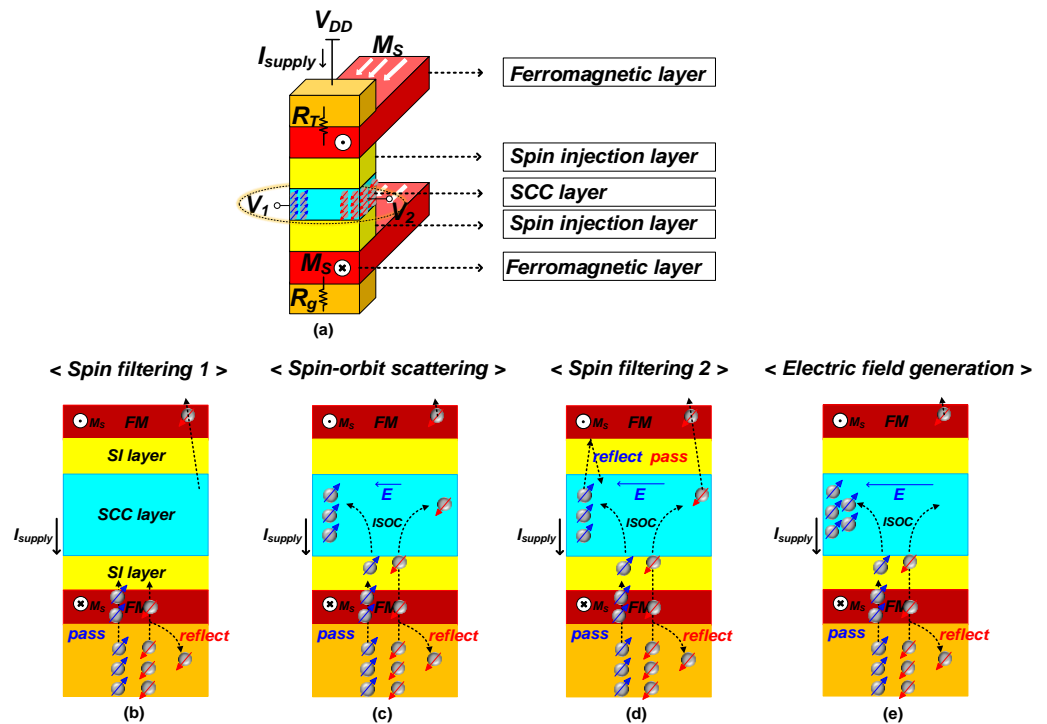


Figure 7. Working principle of the readout structure of the MESO device. (a) Proposed double-FM-layer structure. (b) Spin filtering 1. (c) Spin-orbit scattering. (d) Spin filtering 2. (e) Electric field generation.

The proposed approach is similar to the existing design, with the addition of spin filtering facilitated by an extra FM layer and a spin injection layer. Figure 7b–e show the functionality of the proposed structure, with its operation delineated as follows: upon encountering the first (bottom) FM layer, electrons possessing up-spin orientations selectively propagate through, while those with down-spin orientations are reflected, as shown in Figure 7b. This behavior arises due to the spin-dependent transport properties inherent in ferromagnetic materials. Simultaneously, within the SCC layer, spin-orbit scattering occurs, resulting in a potential difference buildup, as shown in Figure 7c, due to spin-orbit scattering and spin-based filtering effects. Subsequently, these electrons encounter a second (top) FM layer, characterized by an antiparallel magnetization orientation relative to the first

FM layer. Consequently, the second FM layer permits the transmission of electrons with down-spin orientations, while up-spin electrons are filtered out, as depicted in Figure 7d. This arrangement leads to an enhanced difference in densities between electrons with up-spin and down-spin orientations throughout the device. As a result of this improved spin filtering mechanism, there is a notable increase in the output voltage observed at the SCC layer, as illustrated in Figure 7e. This phenomenon underscores the efficacy of utilizing antiparallel magnetization configurations in spintronic devices to manipulate and enhance the spin polarization effect.

In this paper, we specifically explore the potential of employing a double-FM (ferromagnetic)-layer structure in the output portion of the MESO device, providing an alternative to the conventional single FM layer to enhance output charge/voltage. However, the possibilities of this double-FM-layer structure extend beyond the MESO device. Further analysis and research could investigate its application in other advanced spintronic technologies, such as spin Hall nano-oscillators [21,22], where spin-polarized currents are essential to oscillatory behavior. Additionally, exploring its implementation in other materials, such as ferrimagnets [23–25] or Weyl ferromagnets [25–27], could open up new avenues in the development of highly efficient, topologically robust devices. These materials offer unique magnetic properties that could further optimize performance, making this an exciting and promising area for future research.

4. Simulation Results

To validate the functionality of the proposed double-FM-layer structure, we developed and implemented a Verilog-A compact model. We believe that this mathematically precise Verilog-A model is more suitable than the charge-equivalent circuit model for effectively demonstrating the performance of our structure. The charge-equivalent circuit model is limited in that it cannot adequately capture the complex physics underlying the operation of the MESO device. In contrast, the Verilog-A model offers a comprehensive representation of the spin and charge dynamics involved in the device, allowing for a more nuanced evaluation of its behavior. By leveraging the capabilities of the Verilog-A framework, we aim to provide a clearer understanding of how the proposed design can enhance device performance and functionality in practical applications. This approach ultimately strengthens our argument for the efficacy of the double-FM-layer structure in advancing MESO technology.

Our model comprises two components: the FM model and the SCC layer model. The magnetization dynamics of the ferromagnetic (FM) layer are modeled using the Landau–Lifshitz–Gilbert (LLG) equation:

$$\frac{d\mathbf{m}}{dt}(1 + \alpha^2) = -\gamma_0 \mathbf{m} \times (\mathbf{H}_{eff} - \mathbf{T}_f) - \gamma_0 \alpha (\mathbf{m} \times \mathbf{m} \times (\mathbf{H}_{eff} - \frac{\mathbf{T}_d}{\alpha})); \quad (2)$$

$$\mathbf{H}_{eff} = \hat{i} \cdot -N_x m_x + \hat{j} \cdot N_y m_y + \hat{k} [H_k + \frac{2\zeta E_{in}}{t_m \mu_0 M_S} - N_z m_z]; \quad (3)$$

$$\mathbf{T}_d = \eta_d(\theta) \beta (\mathbf{m} \times \mathbf{I}_S \times \mathbf{m}); \quad (4)$$

$$\mathbf{T}_f = \eta_f(\theta) \beta (\mathbf{m} \times \mathbf{I}_S \times \mathbf{m}); \quad (5)$$

$$\beta = \frac{\hbar \gamma}{2q \mu_0 M_S V} \quad (6)$$

where α is the damping constant, representing the rate of energy dissipation during the magnetization's precession, and N_x , N_y , and N_z are the demagnetization factors along the x , y , and z axes, respectively, which account for the shape-dependent internal magnetic field within the material. H_k is the anisotropy field, which describes the magnetic field necessary to overcome the material's inherent magnetic anisotropy. ζ relates to the efficiency with which the applied electric field E_{in} contributes to the magnetization dynamics. The effective

field \mathbf{H}_{eff} incorporates contributions from the external magnetic field, the demagnetizing field, and various internal magnetic interactions, including exchange and anisotropy effects.

For the model of the SCC layer, we used an equivalent representation of the SCC model proposed in [28]. Charge current and spin current calculations are based on the following equations.

For the charge current:

$$I_{\alpha}^c = G_{12}^c \beta_{12,34} (V_3^z - V_4^z) - G_{12}^c \beta_{12,56} (V_5^y - V_6^y) \quad (7)$$

$$I_{\beta}^c = G_{34}^c \beta_{34,56} (V_5^x - V_6^x) - G_{34}^c \beta_{34,12} (V_1^y - V_2^y) \quad (8)$$

$$I_{\gamma}^c = G_{56}^c \beta_{56,12} (V_1^y - V_2^y) - G_{56}^c \beta_{56,34} (V_3^x - V_4^x) \quad (9)$$

Spin current:

$$I_{\alpha}^s = \begin{pmatrix} G_{34}^c \beta_{34,12} (V_3^c - V_4^c) \\ 0 \\ -G_{56}^c \beta_{56,12} (V_1^c - V_2^c) \end{pmatrix} \quad (10)$$

$$I_{\beta}^s = \begin{pmatrix} G_{12}^c \beta_{12,34} (V_1^c - V_2^c) \\ -G_{56}^c \beta_{56,34} (V_5^c - V_6^c) \\ 0 \end{pmatrix} \quad (11)$$

$$I_{\gamma}^s = \begin{pmatrix} 0 \\ -G_{34}^c \beta_{34,56} (V_3^c - V_4^c) \\ G_{12}^c \beta_{12,34} (V_1^c - V_2^c) \end{pmatrix} \quad (12)$$

Table 1 outlines the parameter descriptions and values utilized for performance evaluations. Additionally, I_{supply} was set to 12 mA.

Table 1. Description and values of Verilog-A model parameters.

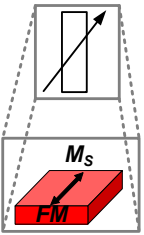
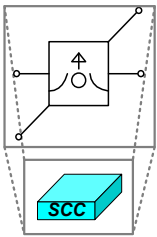
Symbol	Description	Value
< FM layer > 	Saturation magnetization	1.0×10^6 A/m
	Demagnetizing factors	(0, 0, 0.8)
	Damping constant	0.007
	In-plane anisotropy	0
	Polarization efficiency	0.8
	Field-like torque coefficient	0
	VCMA coefficient	60 fJ/V·m
	Initial state (± 1)	+1 for FM 1 and −1 for FM 2
	Magnet thickness	1 nm
	Magnet width	20 nm
	Magnet length	40 nm
	Spin flip length	35 nm
	Conductance	0.5×10^{15} S/m
	Conductance to the perpendicular spin	3.26 S
< SCC layer > 	Conductance	4.0×10^5 S/m
	Spin flip length	1 nm
	Damping constant	0.3
	Layer thickness	1 nm
	Layer width	60 nm
	Layer length	35 nm

Figure 8 illustrates the comparison of the output voltage difference between the previous structure and the proposed structure. The output voltage difference of the proposed structure is 188.49 mV, whereas that of the previous structure is 150.45 mV. Thus, the proposed double spin filtering structure is capable of increasing the output voltage difference (and its corresponding output current) by 25% compared to the previous single spin filtering structure. Although the results did not demonstrate a doubling of the output voltage difference due to the limited mean free path of the spin-polarized current, we believe that further improvements in efficiency can be achieved through material and device engineering.

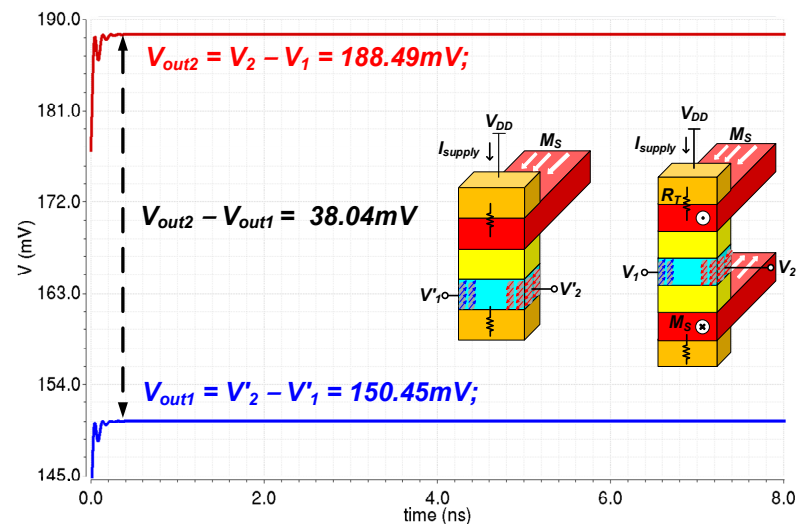


Figure 8. A comparison of the output voltage difference between the previous single spin filtering structure and the proposed double spin filtering structure.

5. Conclusions

In this study, we introduced a comprehensive spin-flow-based explanation of the operational mechanism governing the output section of the MESO device. This framework allowed us to gain deeper insights into the processes that influence charge and voltage generation within the device. Building upon this foundational understanding, we proposed a novel double-FM-layer structure specifically designed to augment the charge and voltage output of the MESO device, ensuring its compatibility with existing CMOS technology. To validate our hypothesis and assess the effectiveness of this new design, we conducted thorough simulations using a Verilog-A compact model-based approach within the Cadence environment. Remarkably, compared to the previous single-FM-layer structure, our proposed design demonstrated a significant enhancement in the output voltage difference, achieving an improvement of 25%. This finding not only underscores the potential of our proposed structure but also highlights its viability as a practical solution in advancing spintronic applications in conjunction with conventional CMOS technology. Overall, our results contribute to the ongoing efforts to optimize MESO devices for next-generation electronic systems and pave the way for further explorations into innovative spintronic architectures.

Author Contributions: Conceptualization, T.N. and B.I.; methodology, T.N.; software, B.I. and S.S.; validation, B.I. and S.S.; formal analysis, T.N.; investigation, B.I.; resources, B.I.; data curation, B.I. and S.S.; writing—original draft preparation, B.I.; writing—review and editing, T.N.; visualization, B.I. and S.S.; supervision, T.N.; project administration, T.N.; funding acquisition, T.N. All authors have read and agreed to the published version of the manuscript.

Funding: This work was supported by the National Research Foundation (NRF) funded by the Korea Government (MSIT) under Grant 2022M3F3A2A01073562.

Data Availability Statement: Data is contained within the article.

Acknowledgments: The EDA tool was supported by the IC Design Education Center (IDEC), Korea.

Conflicts of Interest: The authors declare no conflicts of interest.

References

- Powell, J.R. The Quantum Limit to Moore's Law. *Proc. IEEE* **2008**, *96*, 1247–1248. [CrossRef]
- Nikonov, D.E.; Young, I.A. Overview of Beyond-CMOS Devices and a Uniform Methodology for Their Benchmarking. *Proc. IEEE* **2013**, *101*, 2498–2533. [CrossRef]
- Theis, T.N.; Solomon, P.M. It's Time to Reinvent the Transistor! *Science* **2010**, *327*, 1600–1601. [CrossRef]
- Nikonov, D.E.; Young, I.A. Benchmarking of Beyond-CMOS Exploratory Devices for Logic Integrated Circuits. *IEEE J. Explor. Solid-State Comput. Devices Circuits* **2015**, *1*, 3–11. [CrossRef]
- Manipatrani, S.; Nikonov, D.E.; Lin, C.-C.; Gosavi, T.A.; Liu, H.; Prasad, B.; Huang, Y.-L.; Bonturim, E.; Ramesh, R.; Young, I.A. Scalable energy-efficient magnetoelectric spin-orbit logic. *Nature* **2019**, *565*, 35–42. [CrossRef]
- Seabaugh, A.C.; Zhang, Q. Low-Voltage Tunnel Transistors for Beyond CMOS Logic. *Proc. IEEE* **2010**, *98*, 2095–2110. [CrossRef]
- Rojas-Sánchez, J.-C.; Oyarzún, S.; Fu, Y.; Marty, A.; Vergnaud, C.; Gambarelli, S.; Vila, L.; Jamet, M.; Ohtsubo, Y.; Taleb-Ibrahimi, A.; et al. Spin to charge conversion at room temperature by spin pumping into a new type of topological insulator: α -Sn films. *Phys. Rev. Lett.* **2016**, *116*, 096602. [CrossRef]
- Sinova, J.; Valenzuela, S.O.; Wunderlich, J.; Back, C.H.; Jungwirth, T. Spin hall effects. *Rev. Mod. Phys.* **2015**, *87*, 1213. [CrossRef]
- Rojas-Sánchez, J.C.; Reyren, N.; Laczowski, P.; Savero, W.; Attané, J.P.; Deranlot, C.; Jaffrès, H. Spin pumping and inverse spin Hall effect in platinum: The essential role of spin-memory loss at metallic interfaces. *Phys. Rev. Lett.* **2014**, *112*, 106602. [CrossRef]
- Zhang, S.; Fert, A. Conversion between spin and charge currents with topological insulators. *Phys. Rev. B* **2016**, *94*, 184423. [CrossRef]
- Li, C.; Cai, L.; Wang, S.; Yang, X.; Cui, H.; Wei, B.; Liu, B. Performance Optimization of All-Spin Logic Device Based on Silver Interconnects and Asymmetric Tunneling Layer. *IEEE Trans. Magn.* **2018**, *54*, 1–6. [CrossRef]
- Liang, Z.; Mankalale, M.G.; Hu, J.; Zhao, Z.; Wang, J.-P.; Sapatnekar, S.S. Performance Characterization and Majority Gate Design for MESO-Based Circuits. *IEEE J. Explor. Solid-State Comput. Devices Circuits* **2018**, *4*, 51–59. [CrossRef]
- Liu, H.; Manipatrani, S.; Morris, D.H.; Vaidyanathan, K.; Nikonov, D.E.; Karnik, T.; Young, I.A. Synchronous Circuit Design With Beyond-CMOS Magnetoelectric Spin-Orbit Devices Toward 100-mV Logic. *IEEE J. Explor. Solid-State Comput. Devices Circuits* **2019**, *5*, 1–9. [CrossRef]
- Li, H.; Lin, C.-C.; Nikonov, D.E.; Young, I.A. Differential Electrically Insulated Magnetoelectric Spin-Orbit Logic Circuits. *IEEE J. Explor. Solid-State Comput. Devices Circuits* **2021**, *7*, 18–28. [CrossRef]
- Liang, X.; Chen, H.; Sun, N.X. Magnetoelectric materials and devices. *APL Mater.* **2021**, *9*, 041114. [CrossRef]
- Cherifi, R.O.; Ivanovskaya, V.; Phillips, L.C.; Zbelli, A.; Infante, I.C.; Jacquet, E.; Garcia, V.; Fusil, S.; Bridson, P.R.; Guiblin, N.; et al. Electric-field control of magnetic order above room temperature. *Nat. Mater.* **2014**, *13*, 345–351. [CrossRef]
- Ohno, H.; Chiba, D.; Matsukura, F.; Omiya, T.; Abe, E.; Dietl, T.; Ohno, Y.; Ohtani, K. Electric-field control of ferromagnetism. *Nature* **2000**, *408*, 944–946. [CrossRef]
- Manipatrani, S.; Nikonov, D.E.; Lin, C.-C.; Prasad, B.; Huang, Y.-L.; Damodaran, A.R.; Chen, Z.; Ramesh, R.; Young, I.A. Voltage control of unidirectional anisotropy in ferromagnet-multiferroic system. *Sci. Adv.* **2018**, *4*, eaat4229. [CrossRef]
- Manipatrani, S.; Nikonov, D.E.; Ramesh, R.; Li, H.; Young, I.A. Spin-Orbit Logic With Magnetoelectric Nodes: A Scalable Charge Mediated Nonvolatile Spintronic Logic. 2017. Available online: <https://arxiv.org/abs/1512.05428v2> (accessed on 18 May 2024).
- Mazin, I.I. How to define and calculate the degree of spin polarization in ferromagnets. *Phys. Rev. Lett.* **1999**, *83*, 1427–1430. [CrossRef]
- Kumar, A.; Fulara, H.; Khymyn, R.; Litvinenko, A.; Zahedinejad, M.; Rajabali, M.; Zhao, X.; Behera, N.; Houshang, A.; Awad, A.A.; et al. Robust Mutual Synchronization in Long Spin Hall Nano-oscillator Chains. *Nano Lett.* **2023**, *23*, 6720–6726. [CrossRef]
- Ren, H.; Zheng, X.Y.; Channa, S.; Wu, G.; O'mahoney, D.A.; Suzuki, Y.; Kent, A.D. Hybrid spin Hall nano-oscillators based on ferromagnetic metal/ferrimagnetic insulator heterostructures. *Nat. Commun.* **2023**, *14*, 1406. [CrossRef]
- Zhang, Z.; Zheng, Z.; Zhang, Y.; Sun, J.; Lin, K.; Zhang, K.; Feng, X.; Chen, L.; Wang, J.; Wang, G.; et al. 3D Ferrimagnetic Device for Multi-Bit Storage and Efficient In-Memory Computing. *IEEE Electron Device Lett.* **2021**, *42*, 152–155. [CrossRef]
- Kim, S.K.; Beach, G.S.D.; Lee, K.-J.; Ono, T.; Rasing, T.; Yang, H. Ferrimagnetic spintronics. *Nat. Mater.* **2022**, *21*, 24–34. [CrossRef]
- Chowdhury, N.; Khan, K.I.A.; Bangar, H.; Gupta, P.; Yadav, R.S.; Agarwal, R.; Kumar, A.; Muduli, P.K. Kagome Magnets: The Emerging Materials for Spintronic Memories. *Proc. Natl. Acad. Sci. India Sect. A Phys. Sci.* **2023**, *93*, 477–495. [CrossRef]
- Cheng, E.; Yan, L.; Shi, X.; Lou, R.; Fedorov, A.; Behnami, M.; Yuan, J.; Yang, P.; Wang, B.; Cheng, J.-G.; et al. Tunable positions of Weyl nodes via magnetism and pressure in the ferromagnetic Weyl semimetal CeAlSi. *Nat. Commun.* **2024**, *15*, 1467. [CrossRef]

27. Itoh, S.; Endoh, Y.; Yokoo, T.; Ibuka, S.; Park, J.-G.; Kaneko, Y.; Takahashi, K.S.; Tokura, Y.; Nagaosa, N. Weyl fermions and spin dynamics of metallic ferromagnet SrRuO₃. *Nat. Commun.* **2016**, *7*, 11788. [[CrossRef](#)]
28. Hong, S.; Sayed, S.; Datta, S. Spin Circuit Representation for the Spin Hall Effect. *IEEE Trans. Nanotechnol.* **2016**, *15*, 225–236. [[CrossRef](#)]

Disclaimer/Publisher’s Note: The statements, opinions and data contained in all publications are solely those of the individual author(s) and contributor(s) and not of MDPI and/or the editor(s). MDPI and/or the editor(s) disclaim responsibility for any injury to people or property resulting from any ideas, methods, instructions or products referred to in the content.